NAVAL POSTGRADUATE SCHOOL

MONTEREY, CALIFORNIA

THESIS

ADVANCED QUANTIFICATION OF PLUTONIUM IONIZATION POTENTIAL TO SUPPORT NUCLEAR FORENSIC EVALUATIONS BY RESONANCE IONIZATION MASS SPECTROMETRY

by

Craig T. Lensegrav

June 2015

Thesis Advisor: Craig F. Smith
Co-Advisor: Brett Isselhardt

Approved for public release; distribution is unlimited

THIS PAGE INTENTIONALLY LEFT BLANK

REPORT DOCUMENTATION PAGE

Form Approved OMB No. 0704–0188

1. AGENCY USE ONLY ***(Leave blank)***	**2. REPORT DATE** June 2015	**3. REPORT TYPE AND DATES COVERED** Master's Thesis

4. TITLE AND SUBTITLE
ADVANCED QUANTIFICATION OF PLUTONIUM IONIZATION POTENTIAL TO SUPPORT NUCLEAR FORENSIC EVALUATIONS BY RESONANCE IONIZATION MASS SPECTROMETRY

5. FUNDING NUMBERS

6. AUTHOR(S) Craig T. Lensegrav

7. PERFORMING ORGANIZATION NAME(S) AND ADDRESS(ES)
Naval Postgraduate School
Monterey, CA 93943-5000

8. PERFORMING ORGANIZATION REPORT NUMBER

9. SPONSORING /MONITORING AGENCY NAME(S) AND ADDRESS(ES)
N/A

10. SPONSORING/MONITORING AGENCY REPORT NUMBER

11. SUPPLEMENTARY NOTES The views expressed in this thesis are those of the author and do not reflect the official policy or position of the Department of Defense or the U.S. Government. IRB Protocol number ____N/A____.

12a. DISTRIBUTION / AVAILABILITY STATEMENT
Approved for public release; distribution is unlimited

12b. DISTRIBUTION CODE

13. ABSTRACT (maximum 200 words)

Ongoing work seeks to apply the technology of resonance ionization mass spectrometry (RIMS) to problems related to nuclear forensics and, in particular, to the analysis and quantification of the debris from nuclear detonations. As part of this effort, modeling and simulation methods are being applied to analyze and predict the potential for ionization by laser excitation of isotopes of both uranium and plutonium.

Early work focused on the ionization potential of isotopes of uranium, and the present effort has expanded and extended the previous work by identifying and integrating new data for plutonium isotopes. In addition to extending the effort to this important new element, the work described in this thesis implemented more accurate descriptions of the spatial distribution of the laser beams to improve the accuracy of model predictions compared with experimental results as well as an ability to readily incorporate new experimental data as they become available.

The model is used to estimate ionization cross sections and to compare the relative excitation potential for two isotopes as a function of wavelength, irradiance, and bandwidth.

14. SUBJECT TERMS plutonium, RIMS, model, resonance laser,	**15. NUMBER OF PAGES** 59
	16. PRICE CODE

17. SECURITY CLASSIFICATION OF REPORT	**18. SECURITY CLASSIFICATION OF THIS PAGE**	**19. SECURITY CLASSIFICATION OF ABSTRACT**	**20. LIMITATION OF ABSTRACT**
Unclassified	Unclassified	Unclassified	UU

NSN 7540–01-280-5500

Standard Form 298 (Rev. 2–89)
Prescribed by ANSI Std. 239–18

THIS PAGE INTENTIONALLY LEFT BLANK

Approved for public release; distribution is unlimited

ADVANCED QUANTIFICATION OF PLUTONIUM IONIZATION POTENTIAL TO SUPPORT NUCLEAR FORENSIC EVALUATIONS BY RESONANCE IONIZATION MASS SPECTROMETRY

Craig T. Lensegrav
Lieutenant, United States Navy
B.S.A.T., Thomas Edison State College, 2008

Submitted in partial fulfillment of the
requirements for the degree of

MASTER OF SCIENCE IN APPLIED PHYSICS

from the

NAVAL POSTGRADUATE SCHOOL
June 2015

Author: Craig T. Lensegrav

Approved by: Craig F. Smith
Thesis Advisor

Brett Isselhardt
Co-Advisor

Andres Larraza
Chair, Department of Physics

THIS PAGE INTENTIONALLY LEFT BLANK

ABSTRACT

Ongoing work seeks to apply the technology of resonance ionization mass spectrometry (RIMS) to problems related to nuclear forensics and, in particular, to the analysis and quantification of the debris from nuclear detonations. As part of this effort, modeling and simulation methods are being applied to analyze and predict the potential for ionization by laser excitation of isotopes of both uranium and plutonium.

Early work focused on the ionization potential of isotopes of uranium, and the present effort has expanded and extended the previous work by identifying and integrating new data for plutonium isotopes. In addition to extending the effort to this important new element, the work described in this thesis implemented more accurate descriptions of the spatial distribution of the laser beams to improve the accuracy of model predictions compared with experimental results as well as an ability to readily incorporate new experimental data as they become available.

The model is used to estimate ionization cross sections and to compare the relative excitation potential for two isotopes as a function of wavelength, irradiance, and bandwidth.

THIS PAGE INTENTIONALLY LEFT BLANK

TABLE OF CONTENTS

I. INTRODUCTION....1
A. THE ATOMIC BOMB....2
B. NUCLEAR FORENSICS....4
C. OVERVIEW OF THESIS RESEARCH....7
D. OUTLINE....8

II. RESONANCE IONIZATION MASS SPECTROMETRY....9
A. THE PHYSICS....10
1. Atomic States....10
2. Emission and Absorption....12
a. Angular Momentum and Degeneracy States....13
b. Selection Rules....13
3. Lineshape: Doppler Broadening....14
4. Ionization....15
5. Autoionization....17
B. ISOTOPE FACTORS....18
1. Odd Isotopes....18
2. Even-Odd Effect....19
C. FRACTIONATION IN IONIZING PROCESS....20

III. RATE EQUATION MODEL....21
A. CROSS SECTIONS....23
1. Assumptions....23
2. Transitional Cross Sections for Even and Odd Isotopes....23
B. LASER IRRADIANCE....24

IV. EXPERIMENTAL AND MODEL RESULTS....27
A. TROUBLESHOOTING....27
B. EXPERIMENTAL AND MODEL COMPARISONS....31
C. SUMMARY....34

V. CONCLUSION....35
A. SUMMARY....35
B. FUTURE WORK....36

LIST OF REFERENCES....37

INITIAL DISTRIBUTION LIST....41

THIS PAGE INTENTIONALLY LEFT BLANK

LIST OF FIGURES

Figure 1. Uranium-235 Fission chain reaction, from [1]. 1
Figure 2. Ernest Lawrence prepares his cyclotron in the radiation lab at UC-Berkeley, from [2]....3
Figure 3. Trinity Bomb, 0.053 seconds after detonation, from [1]. 4
Figure 4. Uranium pellet from Find 1, from [4]. 5
Figure 5. Energy level diagrams of two random two-state atoms of different elements, from [8]. 9
Figure 6. Two-state atomic model, from [8]. 10
Figure 7. Lorentzian Function with $\Gamma = 0.2$, from [8]. 11
Figure 8. Generic Ionization Scheme for a multi-step RIMS, from [6]. 16
Figure 9. Plutonium 3-color, 3-photon ionization scheme, from [9]. 16
Figure 10. Autoionization schematic, from [8]. 17
Figure 11. Partial level diagram for even and odd isotopes, from [8]. 19
Figure 12. Atomic parameter inputs into the model for ^{239}Pu and ^{242}Pu. 21
Figure 13. Rate equation model diagram, from [8]. 22
Figure 14. Test 1. Isotope ratio of ^{242}Pu/^{239}Pu vs. wavelength of the second resonance laser at full power. 28
Figure 15. Test 2. Isotope ratio of ^{242}Pu/^{239}Pu vs. wavelength of the second resonance laser with laser power reduced by a factor of ten. 29
Figure 16. Test 3. Isotope ratio of ^{242}Pu/^{239}Pu vs. wavelength of the second resonance laser with laser power reduced by a factor of ten and expanded integration limits. 30
Figure 17. Isotope ratio of ^{242}Pu/^{239}Pu vs. wavelength of the first resonance laser using experimental laser parameters, from [18]. 32
Figure 18. Isotope ratio of ^{242}Pu/^{239}Pu vs. wavelength of the first resonance laser using modeling parameters, from [19]. 32
Figure 19. Isotope ratio of ^{242}Pu/^{239}Pu vs. wavelength of the second resonance laser using experimental laser parameters, from [18]. 33
Figure 20. Isotope ratio of ^{242}Pu/^{239}Pu vs. wavelength of the second resonance laser using modeled parameters. 34
Figure 21. Periodic table of elements, from [26]. Highlighted in red are the isotopes in the actinide series in which we are most interested. 36

THIS PAGE INTENTIONALLY LEFT BLANK

LIST OF TABLES

Table 1. Isotope ratios of plutonium in uranium ammunition, from [6]. 6
Table 2. Selection Rules for Dipole Transitions, from [8]..... 14
Table 3. Parameters used in troubleshooting. Laser power is reduced by a factor of 10 in test 2, while maintaining the same integration limits. Test 3 maintains the reduced laser power, but expands the integration limits. Data was drawn from [18]. 31

THIS PAGE INTENTIONALLY LEFT BLANK

LIST OF ACRONYMS AND ABBREVIATIONS

Am	Americium
amu	Atomic Mass Unit
cm	Centimeter
CW	Continuous Wave
DTRA	Defense Threat Reduction Agency
FWHM	Full Width at Half Maximum
NDRC	National Defense Research Committee
nm	Nanometer
Np	Neptunium
NPT	Treaty of Non-proliferation of Nuclear Weapons
ns	Nanosecond
ps	Picosecond
Pu	Plutonium
RIMS	Resonance Ionization Mass Spectrometry
TIMS	Thermal Ionization Mass Spectrometry
U	Uranium

THIS PAGE INTENTIONALLY LEFT BLANK

ACKNOWLEDGMENTS

Coming to Naval Postgraduate School, I quickly realized I was no longer the proverbial “spring chicken.” Although not ancient by any means, it had been 17 years since I was in an actual classroom environment. I was about to face the most challenging ordeal I had ever encountered, and I didn’t even know it yet. Thankfully, through the efforts of countless hours researching and relearning foreign and not-so-foreign subjects, I achieved what I thought was impossible.

First of all, I would like to express my gratitude to DTRA Basic Research. Through them, this research was possible. Also to Dr. Brett Isselhardt, my thesis co-advisor, who remained patient even as I failed to understand some of the easier concepts. I will be the first to admit my communication skills were marginal at best. However, when needed, you provided me with the assurance of knowing this could be done. Dr. Gamani Karunsari and Dr. Fabio Alves both laid a great foundation for me to start. By pointing me in the right direction, I was able to get started on the right path.

My thesis advisor, Dr. Smith, provided me with infinite guidance. He was able to take a simple mold and transform it into a reputable source of information. Thinking about my decision, I am glad you had the room to facilitate my passion for our nation’s security. There is not a team I would rather be on.

Thank you to my parents for making me who am I today. I know I was not the easiest child to rear, but the time I spent under your roof paved the way for making everything I have ever accomplished possible.

Ana, the love of my life, is the strongest woman I know. She is the true cornerstone of my career. Through the tribulations of deployments and long hours in port, she steadily provided me with the support and love essential for my success. This achievement is not only mine, but hers as well. My children, Craig, Ailana, and Alejandra, are the reason I push hard every day. Learn from my struggles so your life will not be one. Keep on pushing until goals are achieved. And then push some more!

THIS PAGE INTENTIONALLY LEFT BLANK

I. INTRODUCTION

A discovery that happened over Christmas vacation in Vienna, 1938, has had global impacts on the world of nuclear physics [1]. Physicists Lise Meitner and Otto Fritsch were contemplating a finding by Otto Hahn and came across a phenomenon that was previously thought impossible: the splitting of a uranium nucleus. Fission, as Frisch called it, was born.[1] Soon after this discovery—credited also to Fritz Strassman—scientists realized these reactions also emitted secondary neutrons. These secondary neutrons could in turn enable chain reactions, releasing vast amounts of energy (see Figure 1). This energy could be harnessed and used for a virtually endless supply of clean, electrical power. With the world at war, however, more of the focus was directed toward the alternate use of the energy release: the destructive capabilities of nuclear fission and atomic weapons.

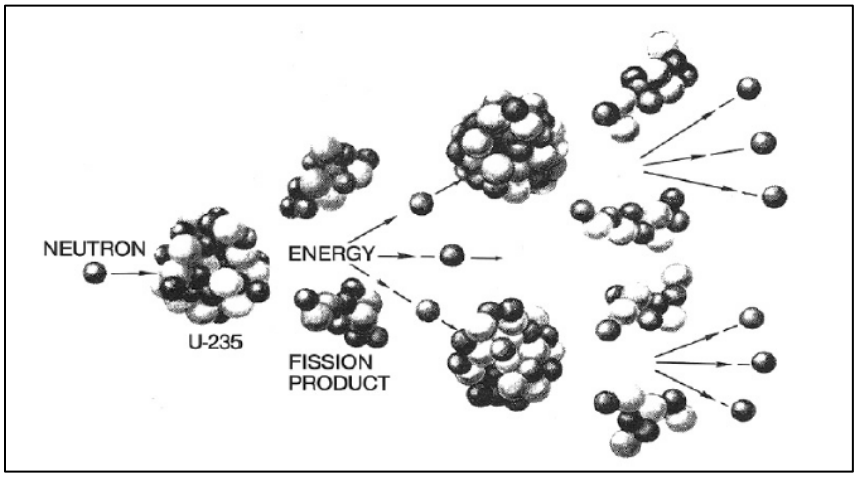

Figure 1. Uranium-235 Fission chain reaction, from [1].

[1] Enrico Fermi had detected fission in 1934, when he began bombarding elements with neutrons, vice the more popular protons, and found the production of new elements. However, he was not fully aware of the implications until after the discovery of the German scientists [1].

A. THE ATOMIC BOMB

The availability of such vast amounts of energy during a period when the world was rapidly approaching global conflict resulted in international scientists' urgent efforts to harness this power and use it to arm their respective nations with a deadly weapon. During the first few years of World War II, Nazi Germany was thought to be in the lead in the nuclear arms race. They had discovered fission in 1934 and from the spring of 1940, had dedicated a large part of the Kaiser Wilhelm Institute in Berlin to uranium research [1].

In the United States, in August of 1939, a letter written by physicist Leó Szilárd in consultation with Edward Teller and Eugene Wigner, and signed by Albert Einstein, was sent to President Franklin D. Roosevelt [1]. The letter discussed the threat that Germany might develop atomic weapons and urged that the United States begin its own nuclear weapons effort [1]. The letter ultimately resulted in the formation of the National Defense Research Committee (NDRC) and the Manhattan Project, in which the scientific community conducted the research in the United States in their own quest for an atomic weapon.

At the time, Ernest Lawrence, a Professor at the University of California and a key player in the Manhattan Project, had been involved in experiments using a cyclotron, as shown in Figure 2. Research involving neptunium revealed that the element decayed into another trans-uranium element [1]. This element was to be known as plutonium. This discovery was crucial because it suggested that there was a possibility of producing large amounts of fissionable plutonium from neutron irradiation of uranium-238, and chemically separating it. The discovery of this phenomenon and the use of plutonium in modern nuclear weapons are important factors of direct relevance to this thesis research.

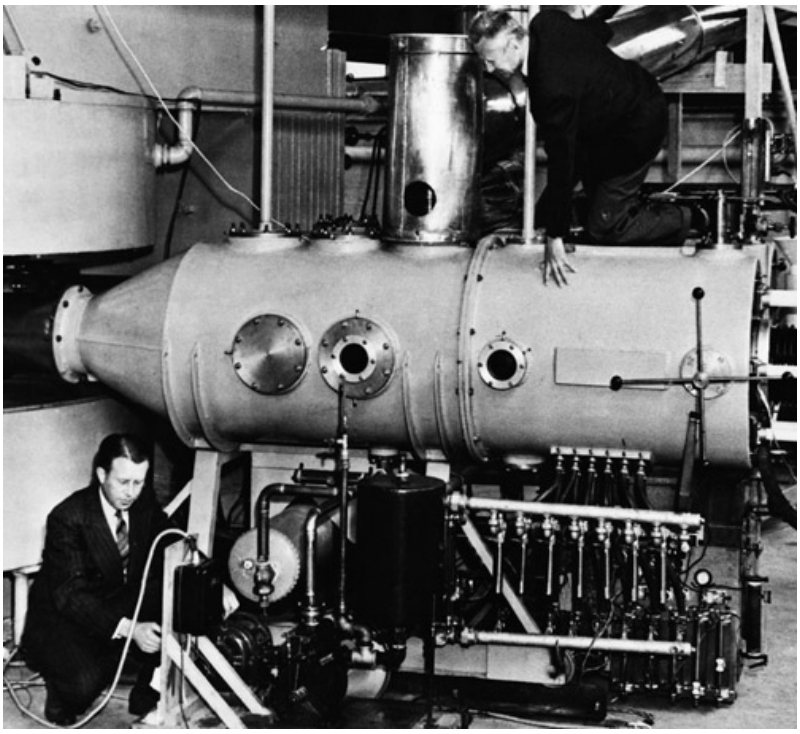

Figure 2. Ernest Lawrence prepares his cyclotron in the radiation lab at UC-Berkeley, from [2].

In April 1945, President Roosevelt passed away, and Vice President Harry Truman ascended to the presidency. Truman was not involved in any of the secrecies associated with the Manhattan Project and therefore had to be thoroughly briefed. In the war, Germany was on the brink of surrender and Japan was being decimated. However, it was a general consensus that Japan would fight to the very end. Some of the American policy makers thought the only way to put an end to the fighting was to deliver the crushing blow of an atomic attack on recognized strategic cities.

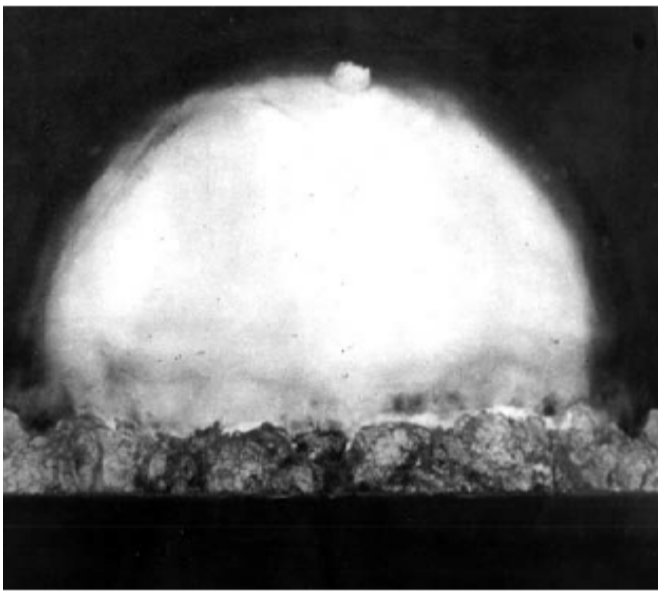

Figure 3. Trinity Bomb, 0.053 seconds after detonation, from [1].

Around the same time, the Americans were preparing to test a plutonium weapon in addition to the uranium bomb that was well developed. The Trinity bomb was detonated on July 16, 1945 [1]. This test meant the United States could now use a second type of bomb against the Japanese. This was true start of the Atomic Age.

B. NUCLEAR FORENSICS

Nuclear forensics is neither a secret technology nor a new one. Records show it dates back to 1949, when samples drawn by the United States from high altitudes off the coast of China proved that Russia had detonated a nuclear device in Central China [3]. However, in more recent times, the nuclear smuggling and trafficking phenomenon has led to the development and improvement of nuclear forensics [3].

Nuclear forensics is a fairly new science, whose modern birth event is considered to be the seizure of Find-1 in Augsburg, Germany, consisting of 72 contraband uranium pellets (see Figure 4) [4]. Standard techniques used to analyze these pellets included: potentiometric titration for determining the uranium content, thermal ionization mass spectrometry (TIMS) for measuring isotropic composition and optical microscopy for determining the macroscopic parameters [4].

Figure 4. Uranium pellet from Find 1, from [4].

If the United States were attacked by a nuclear weapon, questions would arise [5]:

- What is the material in the weapon?
- How bad is the damage? And how much worse will it get?
- Who did it? And did they have help?
- Are there more out there?
- What should I do about it?

These questions must be addressed in the context of an enormous amount of stress and pressure on the President to give the public accurate answers in a short amount of time. These answers will provide the President with information required to make appropriate and decisive decisions.

In the case of plutonium, we know it can be released from various sources, such as nuclear weapon detonations, nuclear processing facilities or reactor accidents [6]. Therefore, isotope ratios can reveal important information in regards to a weapon's origins. Unfortunately, the plutonium concentration can be low in environmental samples of debris, so sensitive testing methods are necessary. Resonance ionization mass spectrometry (RIMS) has been proposed as an alternative or supplement to existing analytical methods to improve our nuclear forensics capabilities [6] and will be described further in Chapter II. An important feature of this technology is its ability to detect ultra-trace amounts of plutonium. As seen in Table 1, the ratios determined by RIMS compare well with previously published values.

Table 1. Isotope ratios of plutonium in uranium ammunition, from [6].

	Fraction of Pu as measured by RIMS [%] (3 σ error)	Fraction in weapon-grade plutonium [%] according to Fetter et al. [4]
Pu-239	93.6(5.9)	93.5
Pu-240	6.2(0.7)	6.0
Pu-241	0.09(0.03)	0.44
Pu-242	0.06(0.01)	0.015

C. OVERVIEW OF THESIS RESEARCH

Ongoing work seeks to apply RIMS technology to problems related to nuclear forensics and, in particular, to the analysis and quantification of debris from nuclear detonations. As part of this effort, modeling and simulation methods are being applied to analyze and predict the potential for ionization by laser excitation of both uranium and plutonium isotopes. Early work focused on the ionization potential of isotopes of uranium, and the present effort has expanded and extended the previous work by identifying and integrating new data for plutonium isotopes. The present work has implemented a more accurate description of the spatial distribution of the laser beams. This will improve the accuracy of model predictions when compared with experiment results. It will also assist in the ability to readily incorporate new experimental data as they become available. The model is used to estimate ionization cross sections and to compare relative excitation on two isotopes as a function of wavelength.

Determining laser power for optimal ionization is crucial for determining the spatial distribution of each of the excited states of the elements of interest. The impact of small shifts in ionization peaks can be overcome by the use of broader band lasers. This will also enable simultaneous and uniform ionization of multiple elements. Careful and detailed understanding of irradiance levels and predicted isotopic responses is required. This research effort has sought to define these levels and explore ways to further refine these results.

Previous efforts were conducted to model the laser ionization potential of isotopes of both uranium and plutonium for potential nuclear forensic applications that involve the use of RIMS to quantify debris from nuclear detonations. The research presented here represents an expansion on that previous work by identifying and integrating new data for plutonium isotopes into our modeling package with the intent of gaining a more accurate representation.

D. OUTLINE

Chapter II introduces RIMS and the physics involved in the process. It also briefly describes isotope shifting and some of the causes. Chapter III introduces the rate equation model. It describes in detail the components of the model. This is use to further understand the relative ionization probability of Pu. It also allows for model testing without using resources which are used experimentally. Chapter IV presents our model results and compares/contrast them with experimental data. Chapter V is the summary of the modeling comparisons. It also provides direction for future research.

II. RESONANCE IONIZATION MASS SPECTROMETRY

Resonance ionization mass spectrometry (RIMS) uses the energy of photons from lasers to excite and ultimately remove an electron from the ground state of an atom [7]. This process starts by creating a cloud of material from a debris specimen by laser desorption. This cloud of material is then subjected to excitation by multiple pulsed lasers finely tuned to excite a transition from one state to the next for the specific elements of interest. The target atoms are then promoted above their ionization threshold and are extracted and sent through a time-of-flight mass spectrometer and counted [7].

As seen in a simplified example in Figure 5, element A has two states: an excited state with non-zero and finite lifetime (given by $\boldsymbol{\tau}$) energy, and a ground state. The probability for finding the excited state at FWHM is given by $\boldsymbol{\Gamma_A}$. If the wavelength ($\boldsymbol{\lambda}$) is close to this energy difference, then the probability of excitation and de-excitation is high. Isselhardt explains, "If the wavelength varies greatly from the energy difference, as seen for element B, then there is a low probability of excitation" [8].

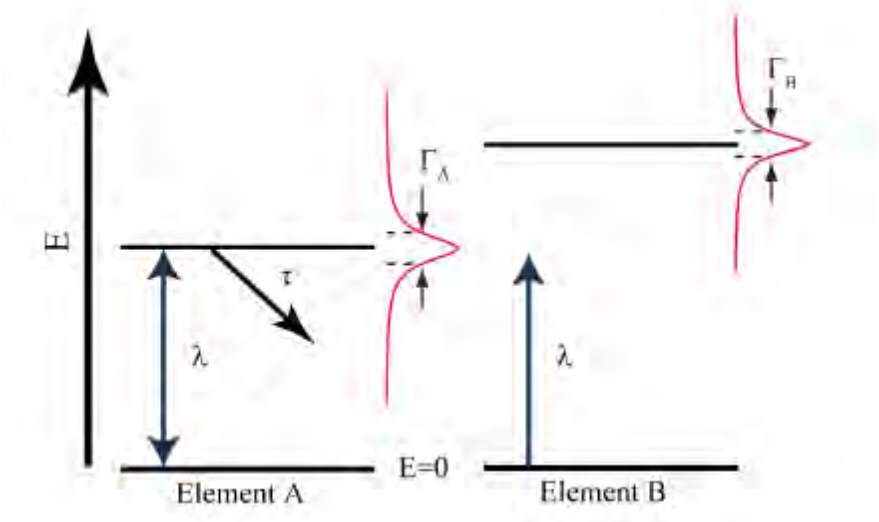

Figure 5. Energy level diagrams of two random two-state atoms of different elements, from [8].

A. THE PHYSICS

The following provides an outline of the physics involved in RIMS. Isselhardt, in [8], provided the foundation for the topic. The following is a summation of his work in both of these references.

1. Atomic States

Two atomic states (Figure 6) can be characterized by the difference in their energies, $E_2 - E_1 = \hbar\omega_0 > 0$. If an atomic state can decay, it must therefore be time-dependent. The time dependent Schrödinger equation can be used to derive the time dependent wave equation Ψ (t). Using the normalized wave function ψ_0, which is stationary in the time independent Schrödinger equation, we can show from [8]

$$\Psi(t) = \Psi_0 \cdot e^{-i\frac{E}{\hbar}t}$$

In its upper state, the atom may decay with an average lifetime τ, where $\tau = \frac{1}{\lambda}$.

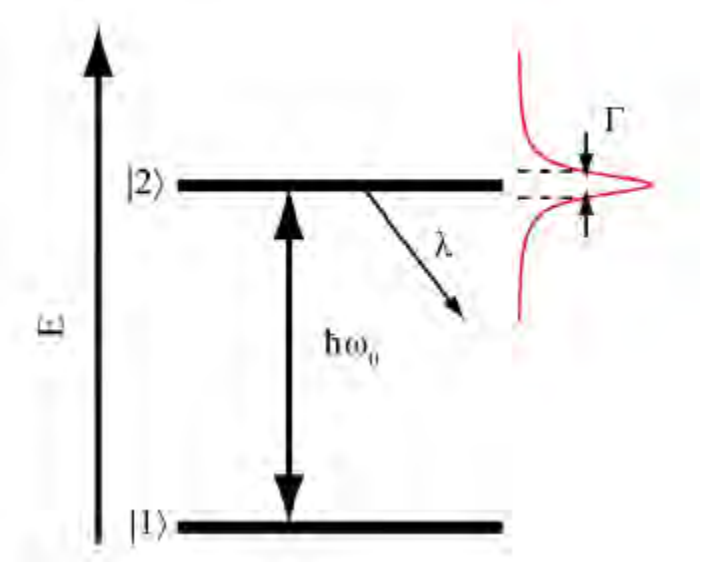

Figure 6. Two-state atomic model, from [8].

If an atomic state can decay, then the probability of it occurring in Ψ is given in [8] by

$$\langle \Psi | \Psi \rangle = e^{-\lambda t}$$

This requires the wave function to be complex. The energy for an atomic state that can decay is defined as $E = E_0 + i\gamma$, -2γ and must equal $\hbar/\tau$, which will be referred to as Γ. This represents the FWHM of the energy distribution about E_0. When it is expressed as a function of angular momentum, Γ becomes $1/\tau$, since $E = \hbar\omega$. The time dependent Schrödinger equation can now be written as

$$\Psi(t) = \Psi_0 \cdot e^{\frac{-i}{\hbar}(E_0 - \frac{i\Gamma}{2})t}$$

The Fourier transform allows us to describe a function of time in terms of frequency. Also, " $E = \hbar\omega$ and $dE = \hbar d\omega$, the probability for finding a time-dependent state in energy is

$$P(E) = \frac{1}{2\pi}\frac{\Gamma}{(E + E_0)^2 + \left(\frac{\Gamma}{2}\right)^2}$$

with P (E) representing a Lorentzian distribution with a FWHM of Γ," shown in Figure 7.

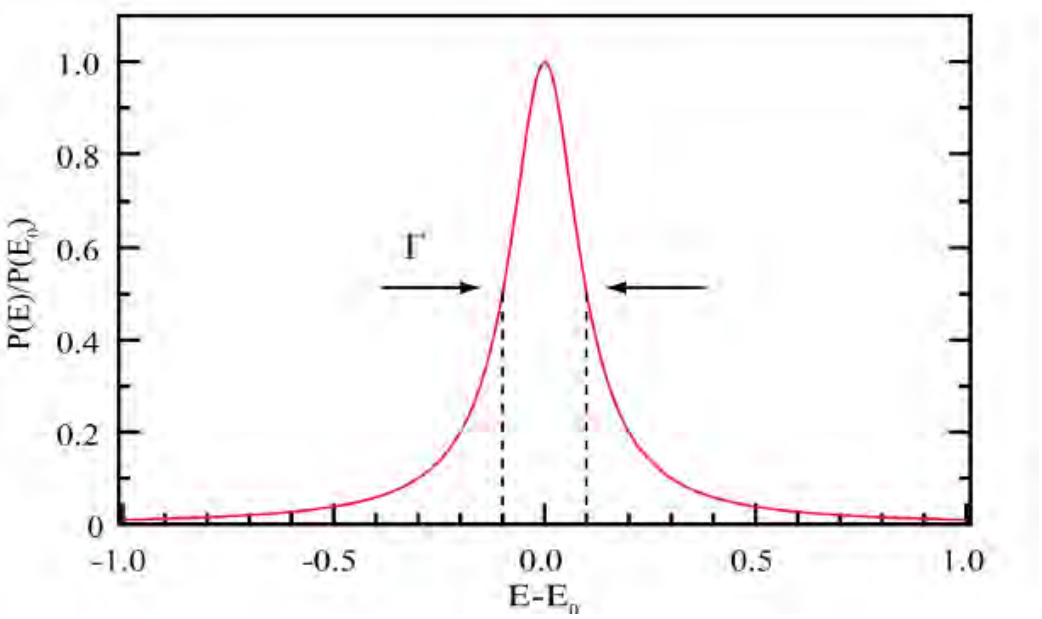

Figure 7. Lorentzian Function with Γ = 0.2, from [8].

2. Emission and Absorption

The line shapes of spontaneous decay and induced emission and absorption are almost identical. Their probability distributions are closely related. The electromagnetic radiation density in a cavity can be described by Planck's distribution and given in [8] as,

$$u(w)\,dw = \frac{u(v)}{2\pi}dv = \left(\frac{\hbar w^3\,dw}{\pi^2 c^3}\right)\left[\frac{1}{\left(e^{\frac{\hbar w}{kT}}-1\right)}\right]$$

Isselhardt describes these variables as "$u(w)\,dw$ is the energy per unit volume, $\hbar$ is the reduced form of Planck's constant, c is the speed of light, k is Boltzmann's constant, and T is temperature in Kelvin" [8]. This equation is legitimate when a balance is reached between energy absorbed at a given frequency by atomic vapor and the energy emitted by the vapor at the same frequency range. These two populations are related by

$$\frac{N_2}{N_1} = \left(\frac{g_2}{g_1}\right)e^{\frac{-\hbar w_0}{kT}}$$

The probability that an atom will either emit a photon into or absorb a photon from a radiation field by decay or emission can be given as

$$\frac{dP_{abs}}{dt} = B_{12}\cdot u_w(w)$$

$$\frac{dP_{emit}}{dt} = B_{21}\cdot u_w(w)$$

$$\frac{dP_{decay}}{dt} = A_{21}$$

According to Isselhardt in, "$u_w(w)$ is the energy density of the radiation field as a function of angular frequency. A_{21}, B_{12}, and B_{21} are Einstein coefficients for decay emission and absorption" [8]. Since state 2 can only decay into state one, A_{21} must equal the inverse of the lifetime of state 2 ($\frac{1}{\tau_2} = \Gamma_2$). Using this knowledge combined with the fact that at thermal equilibrium, these quantities can be expressed as [8]

$$\left(A_{21} + B_{21}\cdot u_w(w)\right)\cdot N_2 = B_{12}\cdot u_w(w)\cdot N_1$$

Substituting Planck's distribution into the equation yields [8]

$$a_w(w) = \frac{A_{21}}{\frac{g_1}{g_2}B_{12}} \frac{1}{\left[e^{\frac{\hbar w}{kT}} - \left(\frac{g_2}{g_1}\frac{B_{21}}{B_{12}}\right)\right]}$$

Comparing this result to Planck's distribution, the relationship for Einstein's coefficients can be derived as follows [8]:

$$g_2 B_{12} = g_1 B_{21}$$
$$A_{21} = \frac{\hbar w}{\pi^2 c^3} \cdot B_{21}$$

a. Angular Momentum and Degeneracy States

Energy degeneracies can be removed in the presence of an electric or magnetic field. However, in thermal equilibrium, the total population of a given level will relate to the number of degenerate states with a level. Using a two state model, this can make things extremely difficult, if we were to consider the degeneracy states of both these levels. All atoms have vast quantities of levels to be considered; therefore accounting for the transitions between these levels must be considered. If we were to consider these transitions as incoherent, we can apply a rate equation approximation. In heavy saturation conditions, from [8], we can use

$$\frac{N_2}{N_1} = \frac{g_2}{g_1}$$

Atoms at each state will now be considered equal to their degeneracy levels, which will be important when a resonance ionization scheme has to be considered.

b. Selection Rules

Conservation of momentum and parity imply there must be rules for each electron transition. The transition dipole matrix is stated in [8] and represented by

$$|Dik|_{\hat{e}} = \hat{e} \cdot e \int \Psi_k^* \vec{r} \Psi_i \, dq$$

When this is equal to zero, it is said the transition is dipole forbidden. Since the parity of the dipole operator is odd, the parity of the wave functions involved in the transition must

be odd. Therefore, the rule of parity came to be known as $\Delta parity = yes$. Other selection rules for dipole transitions are Δ_{m_j} and ΔJ. Their values are listed in Table 2.

Table 2. Selection Rules for Dipole Transitions, from [8].

Component	Rule
Δ_{m_j}	0, ±1
ΔJ	0, ±1(0 to 0 forbidden)
$\Delta parity$	yes

3. Lineshape: Doppler Broadening

Since the atoms are moving in various directions in space, we have to consider they have a frequency v_0 and have a velocity v. These atoms move in a parallel direction of propagation with the laser. A Doppler shift can be expected and is given by [8] as

$$v_D = v_0\left(1 + \frac{\mathrm{v}}{c}\right)$$

Thermalized atom velocities in the gas phase can be described by the Maxwell-Boltzmann probability distribution given by [8] as

$$P(\mathrm{v})\,d\mathrm{v} = \sqrt{\frac{m}{2\pi kT}}\,e^{\frac{-m\mathrm{v}^2}{kT}}\,dv$$

Frequency distribution about v_o is given by [8] as

$$\mathfrak{D}(\mathrm{v}) = \frac{1}{\sqrt{2\pi\sigma}}\,e^{\frac{-(v-v_0)^2}{2\sigma^2}}$$

and is known as a Gaussian distribution with a standard deviation given by [8] as

$$\sigma_v = \sqrt{\frac{kT}{mc^2}}\,v_0$$

This gives the FWHM, or a Doppler width of given in [8] as

$$\Delta v_D = 2 \cdot v_0\sqrt{\frac{2kT \cdot \ln 2}{mC^2}}$$

Using the constant values and converting to wavelength, the following expression is derived in 8 as

$$\Delta\lambda_D = 7.16 \times 10^{-7} \cdot \lambda_0 \cdot \sqrt{\frac{T}{M}}$$

T is in [K] and M is in amu.

4. Ionization

Resonance excitation from the ground state to the final ionization usually requires several intermediate pathways. Possible transitions are pictured in Figure 8. Lifetimes for the first excitation steps last approximately 10ns. The cross-section for absorbing a photon is given by $\sigma = \lambda^2/2\pi$, which is only for an atom at rest. The excitation probability is determined using $dW(t) = \sigma J(t)\, dt$, with $J(t) \approx 10^{18}$ photons/ (cm^2s) and corresponds directly with a power of 100mW/cm^2 [6]. These values easily represent saturation of the first transition. However, according to Wendt in [6], these values represent an ideal situation of constant velocities in all atoms; an effective cross-section must be used. This is the reason direct non-resonant ionization (pathway of the left side of Figure 8) is less than favorable. The cross section provided would be approximately $10^{-17}cm^2$. This process is less than favorable for actinides with complex atomic spectra (plutonium) and can be avoided by heavily populating the auto-ionization state, which is a low-lying state above the ionization potential. This state converts energy into an electron and photon and decays within 1ns. For excitation into the Rydberg state, ionization probability is greatly increased [9].

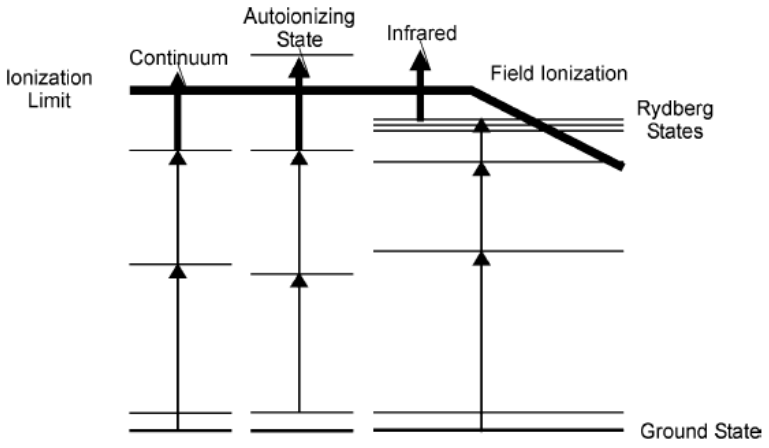

Figure 8. Generic Ionization Scheme for a multi-step RIMS, from [6].

Figure 9 is a partial energy diagram of plutonium showing the ionization scheme of ^{238}Pu and ^{244}Pu. It includes the energy of the levels and the wavelengths of the lasers used to excite the atoms to the next state. This scheme shows plutonium atoms excited from the ground state (E = 0cm^{-1}) to their first excited state, with energy levels of 23765.75 cm^{-1} and 23766.4 cm^{-1} [9]. These atoms are then excited to the second state, to energies of 35568.85 cm^{-1} and 35568.85 cm^{-1} [9]. Finally, they reach ionization through a relatively narrow (6.03eV) auto-ionization state with an energy of 48597.65 cm^{-1} [9].

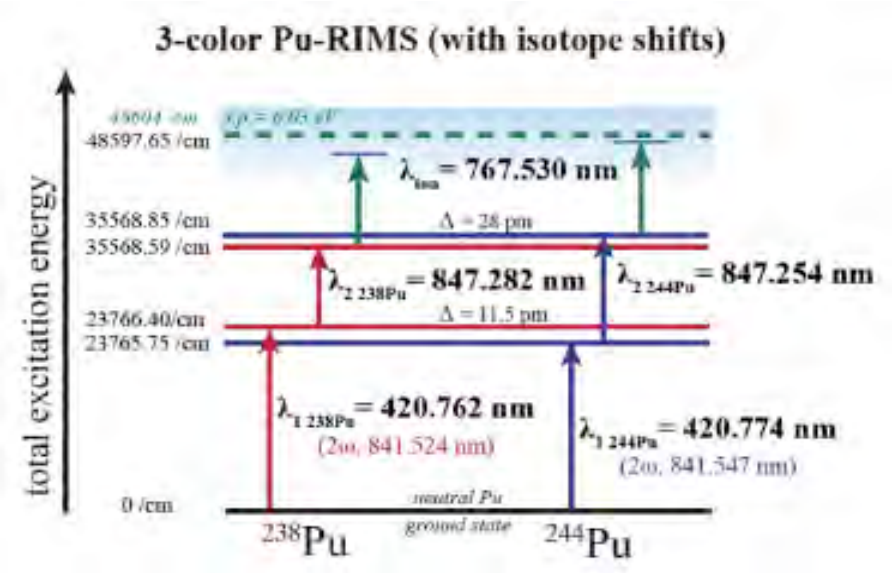

Figure 9. Plutonium 3-color, 3-photon ionization scheme, from [9].

5. Autoionization

Autoionization was first identified by Ugo Fano in 1961 where he describes states involving two excited atoms with E_{Tot} > ionization potential [10]. Atoms in the autoionization state can either decay radiatively to less than the ionization potential or through non-radiative decay by forming an electron and ion. Isselhardt represents this form of decay by $i(n_1 n_2) \rightarrow f(n_3 k)$ and describes the variables as "n_1 is the bound state of the electron and k is the state of the free electron. $i(n_1 n_2)$ is a discrete bound state with E_{Tot} > ionization limit " [8]. Partially, in [10] the width depends on the coupling of states

$$\Gamma_{ai} = 2\pi|\langle i|V|f\rangle|^2$$

and is known as the partial width of decay to the continuum. V is the interaction matrix between the first and final states. Figure 10 gives a generic autoionization process.

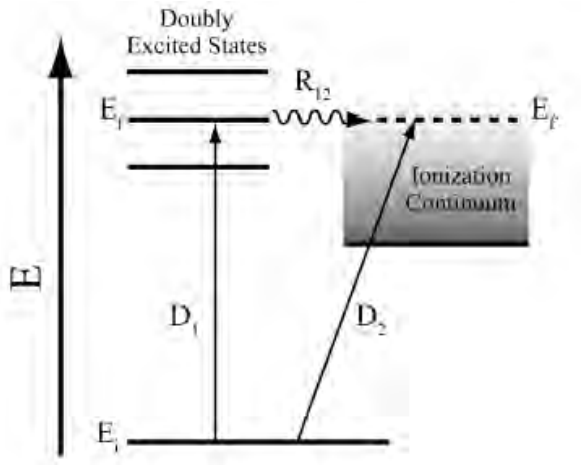

Figure 10. Autoionization schematic, from [8].

Autoionization resonant lineshape (Fano profile) [10] is described by

$$\sigma_{ai}(E) = \sigma_a \frac{(q+\varepsilon)^2}{1+\varepsilon^2} + \sigma_b$$

$$\varepsilon = \frac{2(E-E_0)}{\Gamma}$$

$$q = -\frac{D_1^2}{D_2 R_{12}}$$

Fano defines the variables as "σ_a is the absorption cross section for forming a bound state, σ_b is the cross section for ionization into the continuum, ε is the reduced energy for the doubly excited state, D_1 is the amplitude to the doubly excited state, D_2 is the amplitude to the continuum state, and R_{12} is the transition rate between these states" [10].

B. ISOTOPE FACTORS

Shifting of isotopes is caused by many factors. Two of these will be explored.

The nuclear mass difference factor usually involves the lighter isotopes. According to Isselhardt, it results from the fact that "the additional mass of a neutron is a large part of the total mass. This will lead to a small difference in the mass of a bound electron, which will in turn affect the energy of the excited state" [8].

The volume difference factor is due to the electrical charge distribution for different isotopes and affects the heavier isotopes. Since the atomic mass difference is relatively small compared to the total atomic mass, with each additional neutron, the nuclear radius may see large changes in its nuclear shape. This will subsequently lead to a change in the electric field.

1. Odd Isotopes

Isselhardt explains, "Odd massed nuclei have one unpaired nucleon. Therefore, these nuclei have an angular momentum (I) >0. $I_{nuclear}$ couples with the I of the electrons in its orbit" [8]. The angular momenta of the nuclear (I) and the orbital electron (J) must be coupled into total angular momenta (F).

The left diagram (a) in Figure 11 shows an even isotope with I = 0, s substrate level m_j = 0 and substrate in the upper level m_j = -1, 0, 1. The right diagram (b), shows an odd isotope with the nuclear spin angular momenta of *I = 3/2*. In contrast with the even isotope, there is two states, *F = 3/2* and *1/2* where the energy is shifted by the isotope shift and split by the Casmir formula given in [11] and seen in Figure 11.

$$\Delta E(F) = \frac{A}{2}C + B\frac{3C(C+1) - 4IJ(I+1)(J+1)}{8IJ(2J-1)(2I-1)}$$

$$C = F(F+1) - I(I+1) - J(J+1)$$

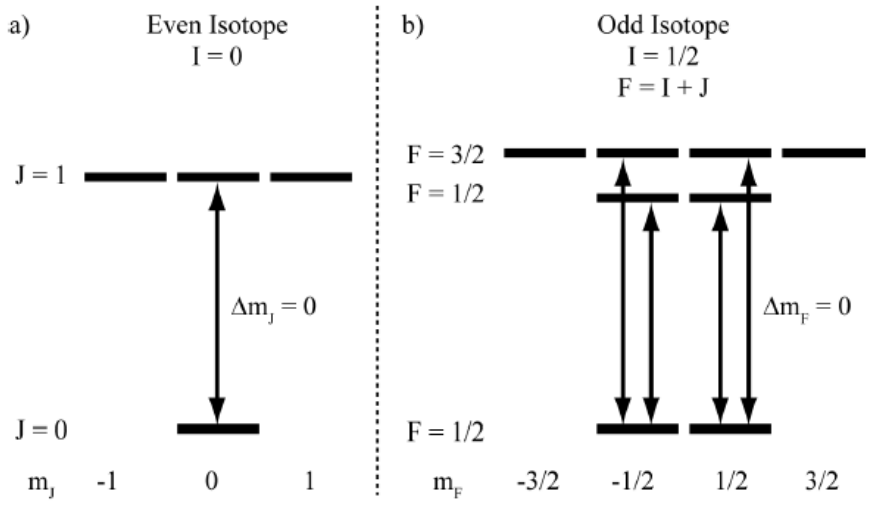

Figure 11. Partial level diagram for even and odd isotopes, from [8].

Substituting m_f for m_j and taking note $\Delta m_f = 0$, we can easily see there are four allowable transitions. Angular momenta differences affect the population rate of each substrate. This will generate differences in the ionization probabilities for both isotopes. Using $\Delta J = +1$ avoids fractionation effects of changes in the selection rules [12].

2. Even-Odd Effect

Peter Lambropoulos and Andreas Lyras were modeling the even-odd isotope ration for tin (Sn) as a function of excitation laser power, when they noticed differences in the ionization probabilities of the even and odd isotopes [13]. However, if the

transitions are saturated, then no differences should be noticed. They accounted for these differences as:

- More states in the odd isotope—the number of states that can be excited by changing the selection rules (*F* instead of *J)*. This will lead to fractionation, increasing the number of atoms that are present during the time of transition saturation.

- Dilution of the oscillator strength.

According to Payne, Allman, and Parks [12], we can overcome the effects of fractionation by:

1. Using fast excitation lasers

2. Changing the bandwidth of the lasers

Both of these methods increase the likelihood of non-resonant ionization of unwanted isotopes. However, if the transitions are sufficiently saturated, these effects can be minimized. Since care must be taken, the cross section of the ionizing laser is kept larger than the excitation lasers, providing the assurance that ions will be formed outside the areas where the ionization process is saturated.

C. FRACTIONATION IN IONIZING PROCESS

The main causes for the discrepancies in ionization probability of isotope ratios are described below:

1. Bandwidth—Isselhardt explains, "Ionization probabilities for isotopes will differ depending on laser irradiance over the resonant cross section" [8].

2. Selection Rules—Angular momentum differences can lead to a divergence in the number of states the isotope can transition to [14].

3. Dynamic Effects—Ionization not saturated can lead to fractionation because the odd isotopes in the excited states when saturate are greater than their even counterparts. Lambropoulos and Lyras in [13] suggest, "Ionization rates may differ due to different angular momentum quantum numbers."

III. RATE EQUATION MODEL

The model that is applied in this research was originally developed to authenticate experimental data resulting from tests performed on isotope ratios to modifications in laser bandwidth. It was used to calculate ionization probabilities of uranium isotopes via a 3-step ionization process, using a variety of input parameters.[2] As seen in Figure 12, the model has been revised to perform these calculations for isotopes of plutonium and other isotopes of interest as prioritized in [15].

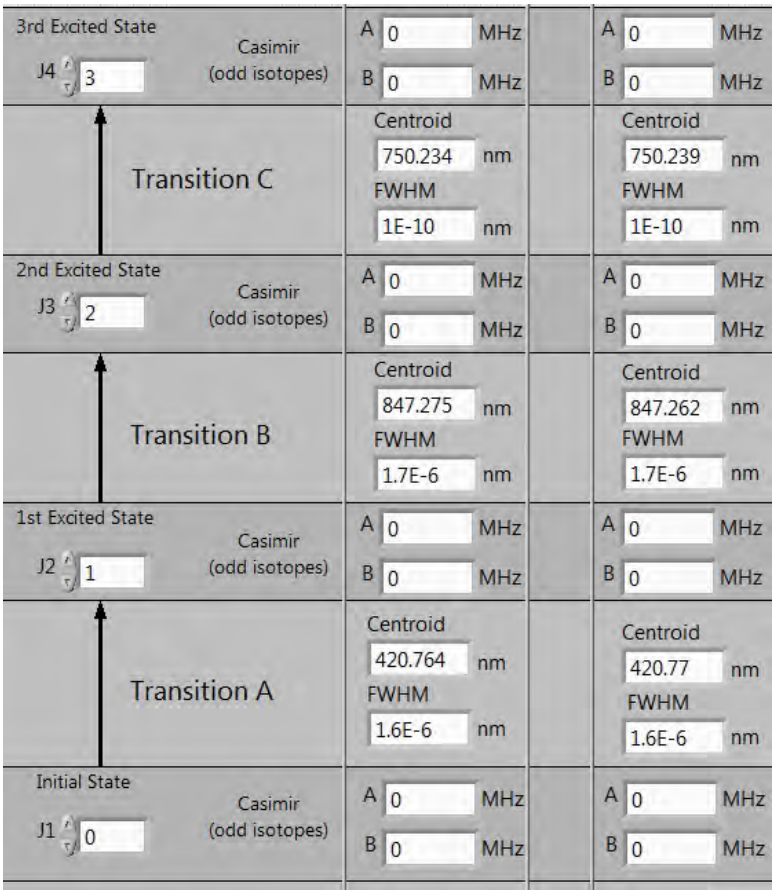

Figure 12. Atomic parameter inputs into the model for ^{239}Pu and ^{242}Pu.

[2] Assumes the atoms are in the ground state.

As shown in Figure 13, the model begins with the calculation of each cross section and laser spectral irradiance for each transition we are attempting to decipher. Once calculated, they are combined considering the time-dependent laser amplitude. This yields, "A time-dependent transition rate. These rates are used to define parameters for the rate equations, which describes the rate change in population of each atomic level" [8]. Upon determination of the parameters, they are integrated over a period of time, and a cumulative fraction of ions is produced. This process can be repeated for the given isotope and iterated over other values.

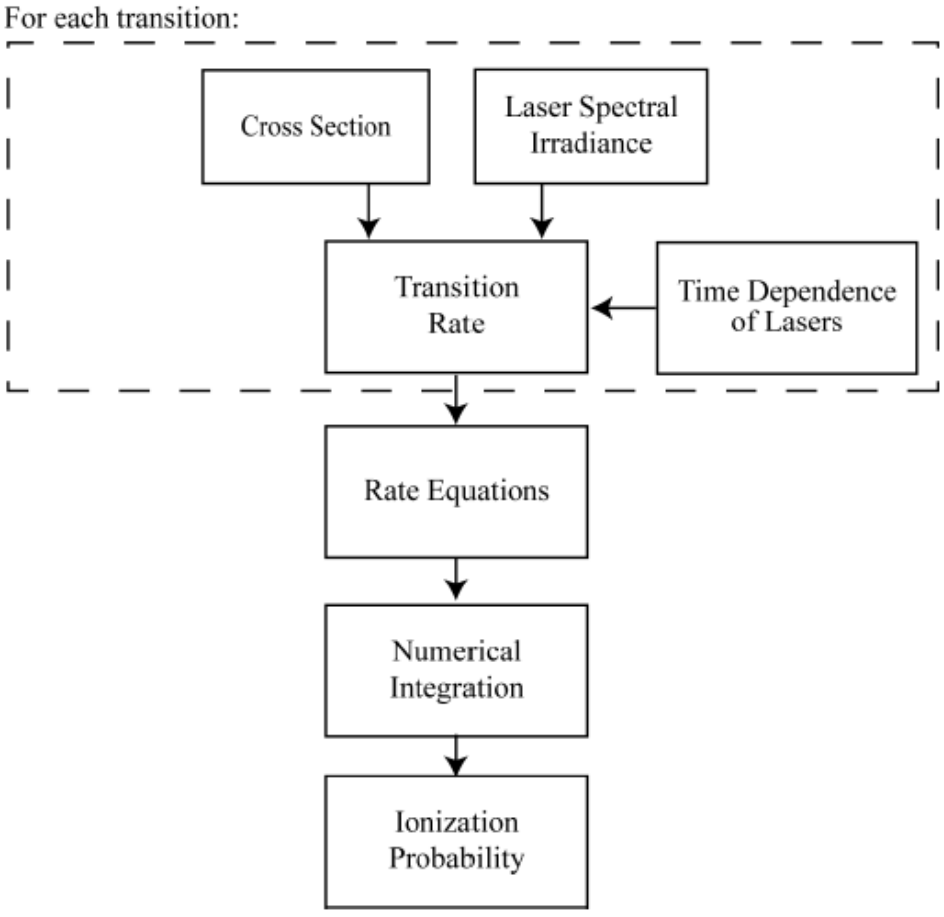

Figure 13. Rate equation model diagram, from [8].

A. CROSS SECTIONS

1. Assumptions

The cross section for absorption can be given in [16] by

$$\sigma m_1 m_2 = \frac{\lambda_0^2}{4} \Gamma_{21} g(w) = \frac{2\pi s(\omega)}{3\varepsilon_0 \hbar \lambda_0} |D_{12}|^2$$

Isselhardt defines the variables as, "λ_o is the mean transition wavelength, Γ_{21} is the partial width of the excited state, $g(w)$ is the normalized lineshape of the transition, and $|D_{12}|^2$ is the squared magnitude of the dipole matrix element for each transition" [8]. This dipole element can be expressed as the product of a reduced matrix element and the Clebsch-Gordan coefficient,[3] per the Wigner-Eckart Theorem [8]

$$\langle J_2, m_2 | D_{even} | J_1, m_1 \rangle = C(J_1, J_2, \Delta J, m_1, m_2, \Delta m) \langle J_2 \| D_{even} \| J_1 \rangle$$

The variables are defined as: "$C(J_1, J_2, \Delta J, m_1, m_2, \Delta m)$ is the Clebsch-Gordan coefficient and $\langle J_2 \| Deven \| J_1 \rangle$ is the reduced matrix element" [8]. The electron spin angular momentum is not affected by the dipole operator.

The even isotopes have equal squares of their Clebsch-Gordan coefficients for each transition between each substrate. In odd isotopes, the transitional energies will not be the same. Using the selection rules stated in Table 2, we can use Wigner-Eckart Theorem and state it as described in [8]

$$\langle F_2, m_2 | D_{odd} | F_1, m_1 \rangle = C(F_1, F_2, \Delta F, m_1, m_2, \Delta m) \langle J_2 \| D_{odd} \| J_1 \rangle$$

$$\langle J_2 \| D_{odd} \| J_1 \rangle = \langle J_2 \| D_{even} \| J_1 \rangle$$

2. Transitional Cross Sections for Even and Odd Isotopes

The model calculates the cross section as a product of amplitude and normalized lineshape. This is given in [8] as

$$\sigma_{12}(\lambda) = \sigma_0 \cdot g(y)$$

[3] Per [17], "Clebsch-Gordan coefficients arise when two angular momenta are combined into a total angular momentum. These coefficients occur when angular momentum from one system is found to have a combination of angular momenta from two subsystems."

where "$\sigma_0 = \frac{\lambda_0^2}{4}\Gamma_{21}$is the peak cross section and $g(y)$is the lineshape for the transition" [8]. This lineshape describes combining the Doppler broadening and width due to spontaneous decay and is the union of Lorentzian with a Gaussian Functions. Therefore, the cross sectional for even isotopes can be given as [16]

$$\sigma_{even} = \frac{\lambda_0^2}{4}\Gamma_{21} \cdot \frac{g_2}{g_1} \cdot [\mathfrak{D}(\lambda) \otimes \mathcal{L}(\lambda)]$$

In odd isotopes, the differences in resonant wavelength of each transition must be accounted for. Isselhardt explains, "The cross section is proportional to the square of the transition dipole and can be multiplied by peak cross section by the squared Clebsch-Gordan coefficient, as

$$\sigma_{m_1 m_2}(\lambda) = \frac{\lambda_0^2}{4}\Gamma_{21} \cdot C(F_1, m_1, F_2, m_2)^2 \cdot g(\lambda)$$

where $C(F_1, m_1, F_2, m_2)^2$ is defined as the squared Clebsch-Gordan coefficient. Since in an odd isotope, the cross section is proportional to the sum of the squared Clebsch-Gordan coefficient for each transition" [8]. The transitional energy differences due to differences in total angular momentum must be taken into account. Therefore from [8],

$$\sigma_{odd} \propto \sum_F D_{odd}^2 = \sum_F \left[\sum_{m_F} [\, C_M(F_1, m_{F1}, F_2, m_{F2})^2] \cdot D_{even}^2 \right]$$

$$= \sum_M C_M(F_1, m_{F1}, F_2, m_{F2})^2 \cdot D_{even}^2$$

B. LASER IRRADIANCE

The spectral irradiance of the laser $I_i(\lambda)$ is a product of photon flux (ϕ_i) and the laser lineshape ($l(\lambda)$)

$$I_i(\lambda) = \phi_i \cdot l(\lambda)$$

Hurst [14] gives the photon flux as

$$\phi_1[photons \cdot cm^{-2}] = (5 \cdot 10^9) \cdot (\lambda_i[nm]) \cdot (P_i[\mu J]) \,/\, A[cm^2]$$

and defines P_i as the pulse intensity, A as the area, and λ_i as the wavelength of the laser beam. These parameters can be varied.

According to Isselhardt, the intensity of a laser beam can be characterized by "Using average total beam energy and spatial distribution in terms of the $1 / e^2$ width" [8]. For normal Gaussian distribution, this width is equivalent to 4σ. Therefore, it can be said half of the population is within ±0.674σ of peak distribution [8]. This area is defined as "$A_{50\%} = \pi \cdot (.674) r_H \cdot (.674) r_v$, where $r_H$and r_v are horizontal and vertical radii. Also, average elliptical area is given by $A_{4\sigma} = \pi \cdot 16 \cdot r_H \cdot r_v$" [8]. Using this knowledge, model predication and experimental results can be compared using the modified laser intensity equation

$$P_{avg} = P_i \cdot 0.5 \cdot \frac{A_{4\sigma}}{A_{50\%}} \cong 17.58 \cdot P_i$$

This takes experimental values of laser intensity and cross sectional area and converts it into average pulse energy (P_{avg}).

During usage, lasers have been known to exhibit variations in mean wavelength, power, position, and timing from pulse to pulse [16]. In order to reproduce the fluctuations in wavelength cause, the model calculates a distribution of ionization probabilities over a designated wavelength range. It then randomly selects samples in this distribution 100,000 times using a normal distribution.

Isselhardt explains, "The model was built around the rate of change in population of atomic level" [8]. It calculates the population density of four states as they are irradiated: ground level, two bound excited states, and finally the ionization level [16]. These four equations are given in [8] as

$$\frac{dN_0}{dt} = W_{01}\left(N_1 - \frac{g_1}{g_0}N_0\right) + \frac{N_1}{\tau_1}$$

$$\frac{dN_1}{dt} = W_{01}\left(\frac{g_1}{g_0}N_0 - N_1\right) + W_{12}\left(N_2 - \frac{g_2}{g_1}N_1\right) - \frac{N_1}{\tau_1} + \frac{N_2}{\tau_2}$$

$$\frac{dN_2}{df} = W_{12}\left(\frac{g_2}{g_1}N_1 - N_2\right) - \frac{N_2}{\tau_2} - W_{2ion}N_2 - W_2N_2$$

$$\frac{dN_{ion}}{dt} = W_{2ion}N_2 + W_{2C}N_2$$

The variables are defined in [8] as: N_1 is the number of atoms in state $|\, i \,\rangle$, W_{ij} is the rate of transition from state $|\, i \,\rangle$ to state $|\, j \,\rangle$, g_i is a degeneracy factor for state $|\, i \,\rangle$, and τ_i is the average lifetime of state $|\, i \,\rangle$. $\pm\, W_{2C}N_2$ terms are added to account for the additional ionization pathways. The negative term accounts for equation of state $|\, 2 \,\rangle$ and the position term accounts for the $|\, ion\rangle$ state [8]. Once the rates W_{ij} are defined by [8] as

$$w_{ij} = \int\int \sigma_{ij}(\lambda) \cdot I_i(\lambda, t)\, d\lambda\, dt \cong \sum_l \sum_k \sigma_{ij}(\bar{\lambda}_k) \cdot I_i(\bar{\lambda}_k, t) \Delta\lambda \Delta t$$

the rate equations can be solved. $\sigma_{ij}(\lambda)$ is the cross section between $|\, i \,\rangle$ and $|\, j \,\rangle$, and $I_i(\lambda, t)$ is spectral irradiance of the laser used to cause the excitation. If a continuous laser was used, we would integrate. Since a pulsed laser is used, we use the summation.

This rate depends on a time variance in the amplitude of the laser pulse. However, this time dependence is independent of wavelength and is expressed in [8] as

$$W_{ij}(t) = w_{ij} \cdot T_i(t)$$

where the variables expression is defined as $T_i(t)$ being the time distribution of the laser pulse [8]. The lineshape is assumed to be Gaussian in nature and is described as [16]

$$T_i(t) = \frac{1}{\sqrt{2\pi\sigma^2}}\, e^{\frac{(t-T_0)^2}{2\sigma^2}}$$

where Isselhardt defines the variables as: σ is the standard deviation and T_0 is the time taken at the peak of the pulse.

IV. EXPERIMENTAL AND MODEL RESULTS

In the effort to use the model to make comparisons with experimental data, some troubleshooting had to occur in order to obtain the correct reference data. A trial and error process was performed on both the first and second resonance laser, but only the second is shown in the description below. Section A documents this troubleshooting process. Table 3 provides a list of all parameters used.

A. TROUBLESHOOTING

The troubleshooting effort consisted of six tests. Three of them are documented here. The tests consisted of a trial by error method of determining the most suitable value of a parameter. They were based on previously known data for both the first and second resonant laser. This process was aimed at determining values for integration limits and laser power, ensuring the end plot was similar to Figure 16.

Figure 14 presents test 1, which is a modeled version of the determination of the $^{242}Pu/^{239}Pu$ ratio vs. wavelength of the second resonance laser. As depicted below, it can be seen that as the laser bandwidth was broadened, the relative lineshape was also broadened. As can be seen in the figure, the results for a bandwidth of 0.001nm are not visible on the plot, which led to further investigation to determine the reason for this.

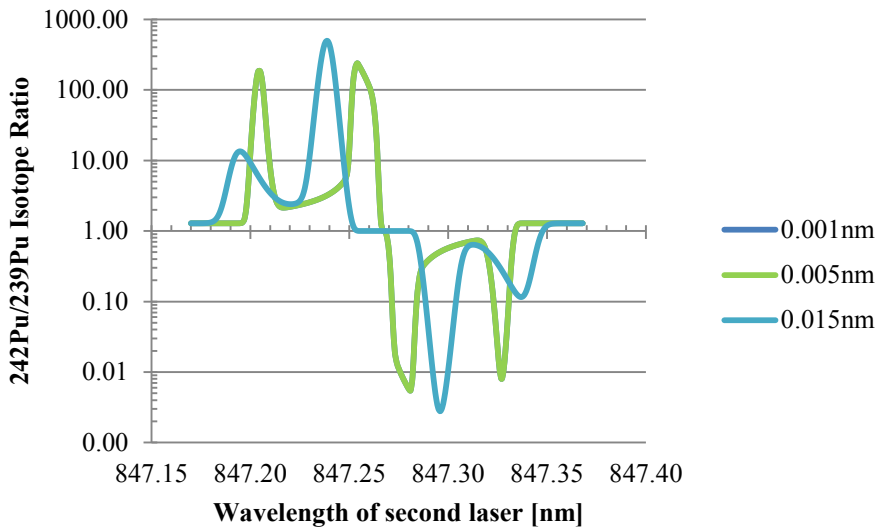

Figure 14. Test 1. Isotope ratio of ^{242}Pu/^{239}Pu vs. wavelength of the second resonance laser at full power.

Figure 15 shows the results for test 2, another modeled version of ^{242}Pu/^{239}Pu ratio vs. wavelength of the second resonance laser. Unlike test 1, test 2 assumed a reduced laser power. The changes from the test 1 results clearly illustrate how laser power effects the calculation of isotope ratio. The lineshape for bandwidth 0.001nm is now visible in this plot. However, the peaks for all bandwidths centered around 847.195nm–847.22nm and 847.32–847.35, appear anomalous and should not be included.

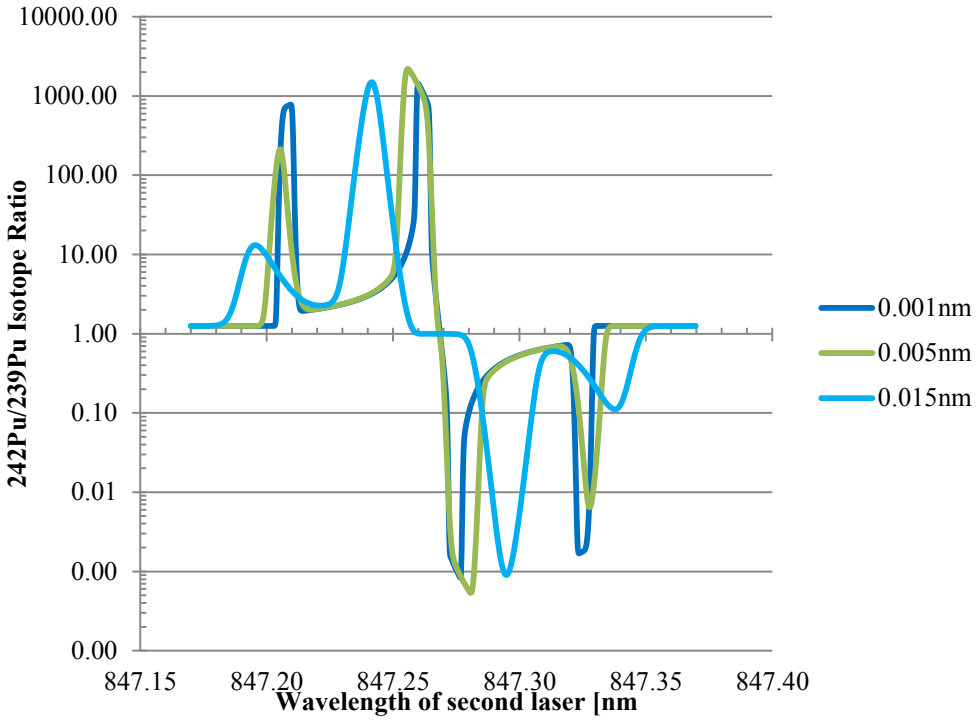

Figure 15. Test 2. Isotope ratio of $^{242}Pu/^{239}Pu$ vs. wavelength of the second resonance laser with laser power reduced by a factor of ten.

Figure 16 presents the results of test 3. Laser power was maintained at its reduced level, but the integration limits inside the model were expanded. As illustrated, the anomalous peaks at the end and beginning of the each bandwidth have disappeared. These line shapes are more representative of what is expected. The values of Table 3, test 3 were used in the remaining tests, except when noted.

This entire process demonstrates the ability of the model to easily troubleshoot and update fields for experimental data, without having to unnecessarily utilize precious resources. Figure 12 displays an example of the fields in which the ability to input a desired value is available.

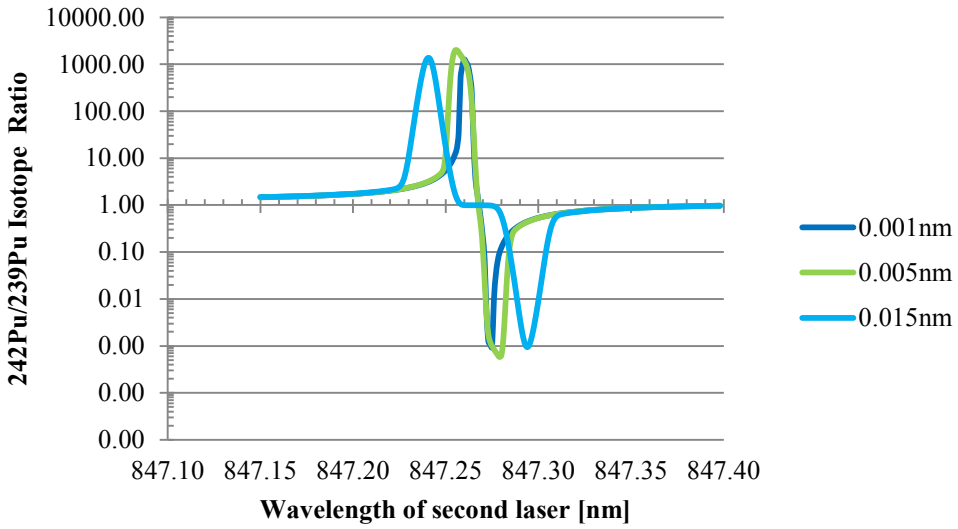

Figure 16. Test 3. Isotope ratio of ^{242}Pu/^{239}Pu vs. wavelength of the second resonance laser with laser power reduced by a factor of ten and expanded integration limits.

Table 3. Parameters used in troubleshooting. Laser power is reduced by a factor of 10 in test 2, while maintaining the same integration limits. Test 3 maintains the reduced laser power, but expands the integration limits. Data was drawn from [18].

Test 1			
Parameter			
Laser Power [mW]			Integration Limits [nm]
First Resonant	Second Resonant	Third Resonant	
1000	656	200	847.15–847.38
Test 2			
Parameter			
Laser Power [mW]			Integration Limits [nm]
First Resonant	Second Resonant	Third Resonant	
100	65.6	20	847.15–847.38
Test 3			
Parameter			
Laser Power [mW]			Integration Limits [nm]
First Resonant	Second Resonant	Third Resonant	
100	65.6	20	847–847.75

B. EXPERIMENTAL AND MODEL COMPARISONS

Figure 17 shows previous experimental results from [18] for three values of laser bandwidth (0.001nm, 0.005nm, and 0.015nm). Figure 18 shows modeled results for the same three bandwidths. In larger bandwidths, the isotopes are saturated in between the peaks. This is not the case for the smaller bandwidths. It is also clear to see that for the

0.015nm bandwidth, the peaks are more symmetric than the 0.001nm bandwidth. According to Isselhardt, this is caused by the fact that "the tails of the isotope not saturated in that wavelength region of the peak become less sensitive to wavelength" [8].

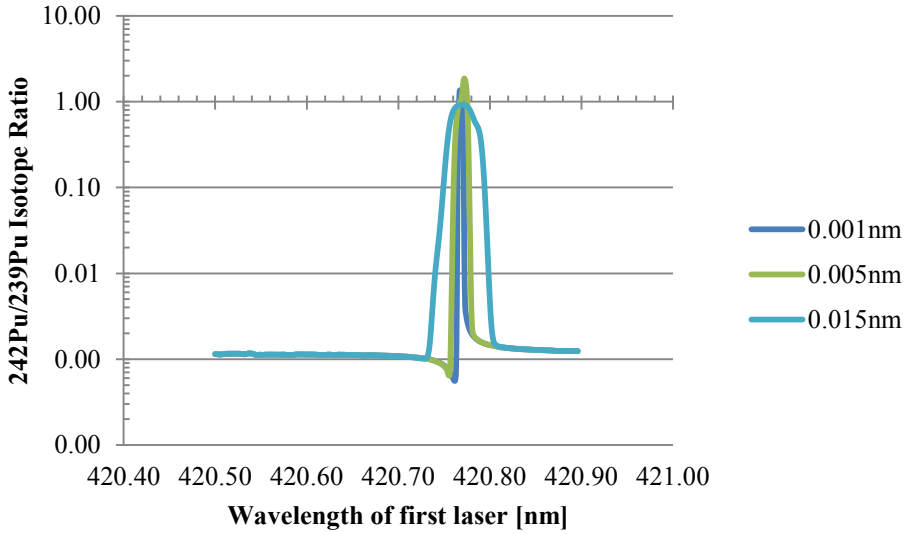

Figure 17. Isotope ratio of $^{242}Pu/^{239}Pu$ vs. wavelength of the first resonance laser using experimental laser parameters, from [18].

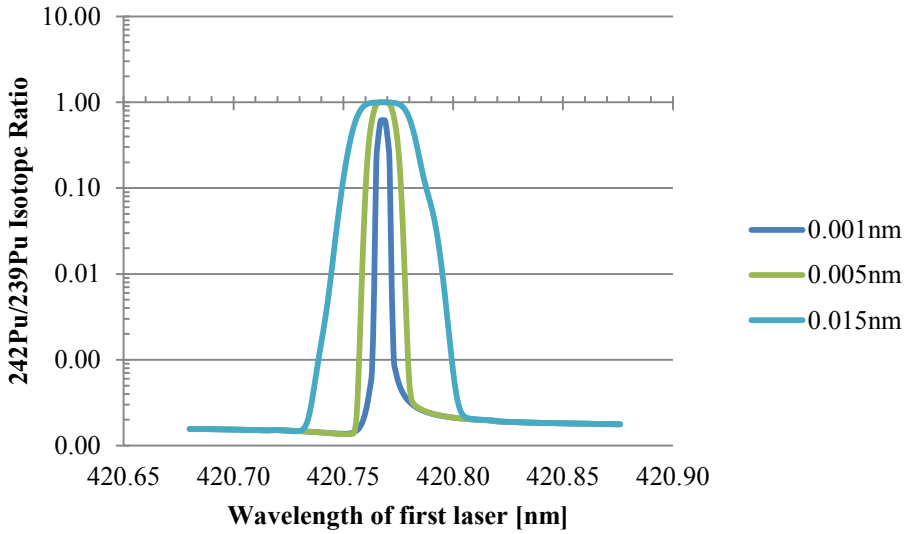

Figure 18. Isotope ratio of $^{242}Pu/^{239}Pu$ vs. wavelength of the first resonance laser using modeling parameters, from [19].

Figure 19 shows additional experimental results from [18] for three values of laser bandwidth (0.001nm, 0.005nm, and 0.015nm). Figure 20 shows modeled results for the same three bandwidths. This indicates an isotope ratio where each resonance is on either side of the peak and they are about equal in amplitude where they cross the y-axis value of one at approximately 847.529nm on Figure 19 and 847.27nm on Figure 20. However, Figure 20 differs from 19 in that each peak's amplitude is approximately a factor of ten larger. It also seems that the peaks for each bandwidth are reversed.

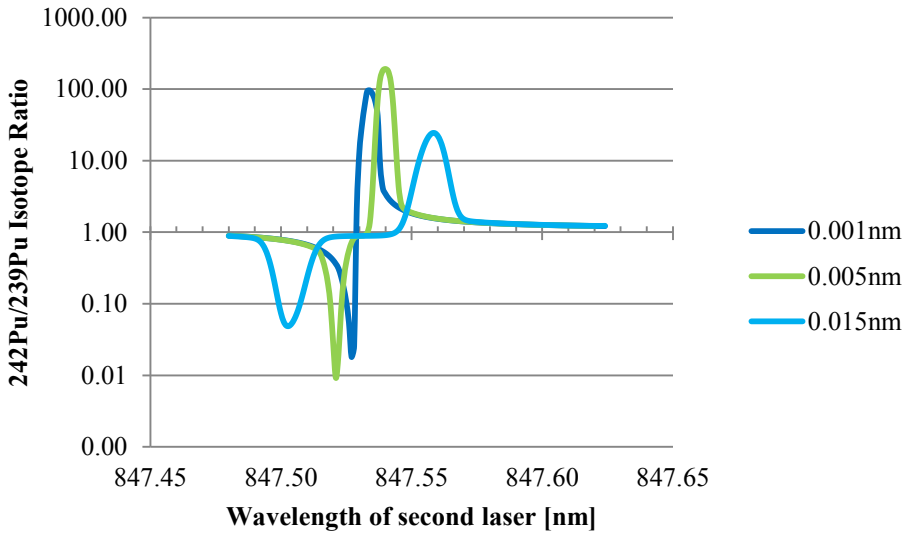

Figure 19. Isotope ratio of ^{242}Pu/^{239}Pu vs. wavelength of the second resonance laser using experimental laser parameters, from [18].

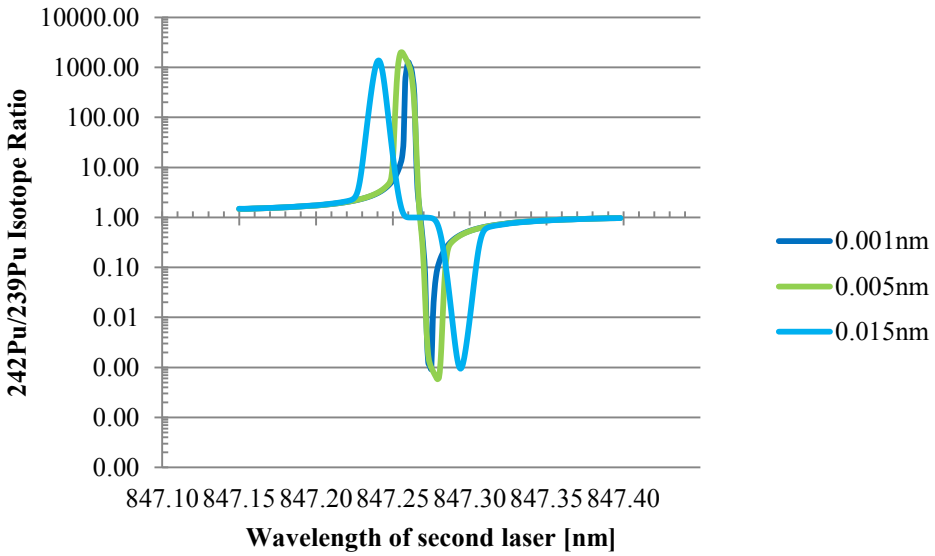

Figure 20. Isotope ratio of ^{242}Pu/^{239}Pu vs. wavelength of the second resonance laser using modeled parameters.

C. SUMMARY

The research in this thesis included a series of troubleshooting tests to provide calibration and understanding of the impact of parameter choices to improve the fidelity of the modeling application. Then it involved exercise of the model to compare outputs to known experimental data to gain important insights into the application of the model to problems of significance to the RIMS nuclear forensics assessment.

V. CONCLUSION

It is believed that 9 countries have nuclear weapons, with others being considered primed for development of such a capability [20]. Each of these nuclear weapons programs has distinguishable characteristics defined by their individual processes. If a nuclear attack were to occur, a most suitable and expeditious method for determining the origin of the device or its nuclear materials is the RIMS technology. There are limited resources for experimental determination of the data needed for RIMS analysis. With that in mind, the rate model equation utilized in this research is established as a necessity. We can use this model to assist in predicting ionization probabilities for many elements and their isotopes, without depleting the reserve of resources.

A. SUMMARY

The research started with a troubleshooting process. It was known how the plot's lineshape should look. Various values of laser centroid, power, and integration limits were chosen until the known plot from experimental data was replicated by modeling results. Such a plot is displayed in Figure 16, with the values of each parameter that resulted from the troubleshooting process in Table 3. Once these values were determined, the comparing and contrasting of experimental and model parameters commenced.

As seen in Figures 17 and 18, the rate equation model was able to sufficiently replicate experimental data. It consistently displayed similar characteristics to what has been seen experimentally for the isotope ratios (^{242}Pu/^{239}Pu) when excited by the first laser wavelength. Displayed in Figures 19 and 20 are the plots of the modeled and experimental laser parameters for the isotope ratio versus wavelength of the second laser. It can be clearly seen that a disagreement between model and experimental data is present. This indicates that more research is necessary in order to reproduce acceptable isotope ratios for the second resonance laser wavelengths. However, this is not considered to detract from the present research; it implies that the best way to interpret and utilize the model predictions is to compare the results to more precise experimental data and continue the process of fine tuning the model.

B. FUTURE WORK

In Figure 21, the period table's actinide series elements have been highlighted. Per [15], americium (Am) and neptunium (Np) are the next elements to be researched. Both elements "are primarily formed from the decay of Pu and U" [15]. Understanding these elements and how their isotopes are formed will assist in determining the fuel isotopes and where the fuel was manufactured. Np ([21], [22]) and Am ([23]–[25]) have already had preliminary studies to determine some of the parameters. However, in order to fully experiment, further research is required to gain key parameters.

Work is also being conducted to substitute one of the pulsed lasers with a continuous wave (CW) laser. It would be beneficial to re-run some of the experiments on U and Pu with the new laser implemented. Running the model based on the parameters of the CW laser would be valuable in validating and understanding the experiments.

PERIODIC TABLE OF THE ELEMENTS

1 H 1.0079																	2 He 4.0026
3 Li 6.941	4 Be 9.012											5 B 10.811	6 C 12.011	7 N 14.007	8 O 16.00	9 F 19.00	10 Ne 20.179
11 Na 22.99	12 Mg 24.30											13 Al 26.98	14 Si 28.09	15 P 30.974	16 S 32.06	17 Cl 35.453	18 Ar 39.948
19 K 39.10	20 Ca 40.08	21 Sc 44.96	22 Ti 47.90	23 V 50.94	24 Cr 52.00	25 Mn 54.938	26 Fe 55.85	27 Co 58.93	28 Ni 58.69	29 Cu 63.55	30 Zn 65.39	31 Ga 69.72	32 Ge 72.59	33 As 74.92	34 Se 78.96	35 Br 79.90	36 Kr 83.80
37 Rb 85.47	38 Sr 87.62	39 Y 88.91	40 Zr 91.22	41 Nb 92.91	42 Mo 95.94	43 Tc (98)	44 Ru 101.1	45 Rh 102.91	46 Pd 106.42	47 Ag 107.87	48 Cd 112.41	49 In 114.82	50 Sn 118.71	51 Sb 121.75	52 Te 127.60	53 I 126.91	54 Xe 131.29
55 Cs 132.91	56 Ba 137.33	57 *La 138.91	72 Hf 178.49	73 Ta 180.95	74 W 183.85	75 Re 186.21	76 Os 190.2	77 Ir 192.2	78 Pt 195.08	79 Au 196.97	80 Hg 200.59	81 Tl 204.38	82 Pb 207.2	83 Bi 208.98	84 Po (209)	85 At (210)	86 Rn (222)
87 Fr (223)	88 Ra 226.02	89 †Ac 227.03	104 Rf (261)	105 Db (262)	106 Sg (266)	107 Bh (264)	108 Hs (277)	109 Mt (268)	110 Ds (271)	111 Rg (272)	112 § (277)	§Not yet named					

*Lanthanide Series	58 Ce 140.12	59 Pr 140.91	60 Nd 144.24	61 Pm (145)	62 Sm 150.4	63 Eu 151.97	64 Gd 157.25	65 Tb 158.93	66 Dy 162.50	67 Ho 164.93	68 Er 167.26	69 Tm 168.93	70 Yb 173.04	71 Lu 174.97
†Actinide Series	90 Th 232.04	91 Pa 231.04	92 U 238.03	93 Np 237.05	94 Pu (244)	95 Am (243)	96 Cm (247)	97 Bk (247)	98 Cf (251)	99 Es (252)	100 Fm (257)	101 Md (258)	102 No (259)	103 Lr (262)

Figure 21. Periodic table of elements, from [26]. Highlighted in red are the isotopes in the actinide series in which we are most interested.

LIST OF REFERENCES

[1] F.G. Gosling, "The Manhattan Project: Making of the atomic bomb," United States Department of Energy, Washington, DC, DOE/MA-0002. Revised, Jan. 2010, pp. 4–72.

[2] T. Long. (2008, February 20). A huge step toward atomic energy. *Wired* [Online]. Available: http://archive.wired.com/science/discoveries/news/2008/02/dayintech_0220

[3] K. Mayer *et al*., "Nuclear forensics-a methodology providing clues on the origin of illicitly trafficked nuclear materials," *The Analyst*, vol. 130, no. 4, 2004, pp. 433–441.

[4] K. Mayer *et al*., "Nuclear forensic science-from cradle to maturity," *J. of Alloys and Compounds,* vols. 444–445, Oct. 2007, pp. 50–56.

[5] Committee on Nuclear Forensics and National Research Council, *Nuclear Forensics: A Capability at Risk,* Washington, DC, Nat. Academies Press, 2010.

[6] K. Wendt, N. Trautmann, "Recent developments in isotope ratio measurements by resonant ionization mass spectrometry," *Int. J. of Mass Spectrometry,* no. 242, pp. 161–168, 2005.

[7] C. Lensegrav *et al*., "Advanced quantification of plutonium ionization potential to support nuclear forensic evaluations by resonance ionization mass spectrometry (RIMS)," presented at American Physical Society 2015 March Meeting, San Antonio, TX, 2015.

[8] B. Isselhardt, "Quantifying uranium isotopes using resonance ionization mass spectrometry: the influence of laser parameters on relative ionization probability," Ph.D. dissertation, Dept. Nucl. Eng., Univ. California, Berkeley, 2011.

[9] K. Knight *et al*., "Multi-actinide isotropic measurements from a single sample by resonance ionization mass spectrometry," presented at Institute of Nuclear Materials Management, Palm Desert, CA, 2011.

[10] U. Fano, "Effects of configuration interaction on intensities and phase shifts," *Physical Review,* vol. 124, no. 6, pp. 1866–1978, Dec. 1961.

[11] P.G. Schumann *et al*., "High-resolution triple-resonance autoionization of uranium isotopes." *Spectrochimica Acta part B: Atomic Spectroscopy.* vol. 60, no. 11, pp. 1402–1411, Aug. 2005.

[12] M.G. Payne and S.L. Allman, "Effect of hyperfine structure on ionization efficiencies in stepwise ionization using broad bandwidth lasers," *Spectrochimica Acta Part B*, vol. 46B, no. 11, pp. 1439–1457, May 1991.

[13] P. Lambropoulos, A. Lyras, "Theory of resonant ionization by broad-band radiation in the determination of isotropic abundances," *Physical Review A,* vol. 40, no. 4, pp. 2199–2202, Aug. 1989.

[14] M.G. Hurst and G.S. Payne, *Principles and Applications of Resonance Ionization Spectroscopy*, London: CRC Press, 1988.

[15] K.B. Knight *et al*., "Prioritization study of elements relevant to RIMS counter-WMD," LLNL, Livermore, CA, TR-652515, Mar. 2014.

[16] B.H. Isselhardt *et al.*, *"*Relative Ionization Probabilities for resonance ionization mass spectrometry: the influence of laser induced bias on uranium isotope ratios," unpublished.

[17] V. P. Krainov, "Appendix B: Clebsch-Gordan coefficients," in *Radiative Processes in Atomic Physics,* 1st ed. Hoboken, NJ: Wiley & Sons, 1997

[18] B.H. Isselhardt. Unpublished results (2015).

[19] B.H. Isselhardt and C.T. Lensegrav. Unpublished results (2015).

[20] J. Simrin. (2014, September 17). What countries have nuclear weapons? *Testtube Daily Show* [Online]. Available: http://testtube.com/testtubedailyshow/what-countries-have-nuclear-weapons/

[21] S. Raeder *et al.,* "Determination of the 3 step excitation and ionization scheme of 237-Np for trace analysis of RIMS." *Spectrochimica Acta part B: Atomic Spectroscopy.* vol. 66, no. 3–4, pp. 242–247, Mar.–Apr. 2011.

[22] J. Riegel *et al.,* " Resonance Ionization Mass Spectrometry for trace analysis of neptunium." *Applied Physics B: Photophysics and Laser Chemistry.* vol. 56, pp. 275–280, Feb 1993

[23] R. Deissenberger *et al.*, " First determination of the ionization potential of americium and curium." *Angewandte Chemie International Edition in English.* vol. 34, no. 7, pp. 814–815, Apr. 1995.

[24] S. Köhler *et al.,* "Determination of the first ionization potential of actinide elements by resonance ionization mass spectrometry." *Spectrochimica Acta part B: Atomic Spectroscopy.* vol. 52, no. 6, pp. 717–726, Jun 1997.

[25] V. Fivet *et al.,* "Transition probabilities in complex ions: the case for americium." *Journal of Electron Spectroscopy and Related Phenomena,* vol. 156–158, pp. 255–258, 2007.

[26] SAT subject test practice: Chemistry. (n.d.). *Scholastic Aptitude Test*. [Online]. Available: https://sat.collegeboard.org/practice/sat-subject-test-preparation/chemistry

THIS PAGE INTENTIONALLY LEFT BLANK

INITIAL DISTRIBUTION LIST

1. Defense Technical Information Center
   Ft. Belvoir, Virginia

2. Dudley Knox Library
   Naval Postgraduate School
   Monterey, California